Reprinted from the Journal of the American Ceramic Society, Vol. 73, No. 6, June 1990

journal

J. Am. Ceram. Soc., 73 [6] 1548–54 (1990)

Three-Dimensional Effects in Microcrack Nucleation in Brittle Polycrystals

Fariborz Ghahremani and John W. Hutchinson*

Division of Applied Sciences, Harvard University, Cambridge, Massachusetts 02138

Viggo Tvergaard

Department of Solid Mechanics, The Technical University of Denmark, DK-2800 Lyngby, Denmark

Stress concentration at vertices where grains of a polycrystal meet at a point is contrasted with stress concentration at two-dimensional junctions where grains join along a line. Effects of thermal anisotropy and elastic anisotropy orientation mismatches from grain to grain are considered. Special geometries with moduli mismatches are also analyzed to shed light on three-dimensional vs two-dimensional behavior. Although there are exceptions, it is generally found that the stress concentration at vertices is more singular than that at junctions. Singularities which are stronger than cracklike singularities (i.e., stress $\propto r^{-s}$ where $s > 1/2$) are found, and the implication of such "super singularities" for microcrack nucleation is discussed. Conditions for propagation of microcrack flaws at vertices are analyzed and contrasted with those at junctions. [Key words: microcracking, nucleation, polycrystalline materials, grains, anisotropy.]

I. Introduction

This paper summarizes a study of the three-dimensional (3D) stress distributions in the vicinity of vertices where grains of a polycrystal meet at a point. The study contrasts behavior at vertices with that at two-dimensional (2D) junctions where grains meet along a line. In particular, the study addresses the question whether the stresses responsible for nucleating microcracks are more severe at vertices or at junctions. Residual stresses and stresses due to an overall applied stress are determined in the presence of both elastic anisotropy mismatch (i.e., grains with a given elastic anisotropy but different orientation meeting at a vertex or junction) and thermal expansion anisotropy mismatch. Energy release rates for microcrack flaws at a vertex or junction are also computed and contrasted.

Studies of microcrack nucleation in brittle polycrystals have been confined largely to 2D models. Thermal expansion mismatch leads to logarithmically singular residual stresses at junctions when the elastic properties are taken to be isotropic and identical from grain to grain. Junctions are therefore likely sites for microcrack nucleation, and the consequence of introducing cracklike flaws at a junction has been analyzed.[1-3] Estimates have been obtained for the relation between the intrinsic flaw size and the critical grain size—the largest grain size which can survive a given temperature drop below the fabrication temperature.[4] More recently it has been shown that elastic anisotropy of the grains can bring about even more severe stress conditions at a 2D junction.[5] Elastic anisotropy mismatch induces stress singularities at a junction of the form $\sigma \sim r^{-s}$, where the order s depends on the degree of anisotropy and relative orientations of the grains. In general, this singularity is dominant and determines the stress variation in the immediate vicinity of the junction whether the stress is due to thermal expansion mismatch or applied stress. Elastic anisotropy and thermal expansion mismatches working together lower the critical grain size below the predictions based on thermal expansion mismatch alone.

In this paper we produce and examine a number of special solutions to 2D and 3D problems to gain insight into the severity of stressing at 3D vertices vs 2D junctions. The following are brief statements of the findings in each section of the paper.

Section II: Stressing is somewhat more severe at a junction than a vertex when the elastic moduli are isotropic and homogeneous with stressing due only to thermal expansion mismatch.

Section III: Stress singularities at a vertex are modeled using axisymmetric conical geometries with elastic moduli mismatch and elastic anisotropy mismatch. Generally, the order of the singularity is significantly stronger at a vertex than at the corresponding 2D junction. The possibility and implications of super singularities, where the stresses at the vertex are more singular than $r^{-1/2}$, are noted.

Section IV: The order s of the dominant stress singularity is determined using a special numerical method for true 3D vertices with elastic anisotropy mismatch, i.e., where grains of a given anisotropy but differing orientation meet at a point. Here, too, the calculations suggest that a vertex is likely to be more critical than a junction.

Section V: Energy release rates for microcrack flaws at vertices and junctions are computed and compared. The calculations are carried out on 2D and 3D geometries using a finite-element method. Thermal expansion mismatch and elastic moduli mismatch or elastic anisotropy mismatch are taken into account. Stressing due to temperature change and applied overall load is considered with findings which are consistent with the singularities found in Section III.

II. Thermal Expansion Mismatch with Homogeneous, Isotropic Moduli

Evans[2] and Fredrich and Wong[3] have determined the residual stress distributions for several 2D, plane strain geometries chosen to model grains in a polycrystal. Their examples display a logarithmic singularity in the stresses at the junction where three or more grains with identical isotropic elastic moduli meet with mismatches in thermal expansion coefficients. Here we give two general asymptotic results for the stress in the immediate vicinity of a junction and a vertex for the single wedge geometries shown in Fig. 1.

A. Evans—contributing editor

Manuscript No. 198338. Received June 7, 1989; approved November 27, 1989.

Supported by the National Science Foundation under Grant No. MSM-88-12779, by the Materials Research Laboratory under Grant No. NSF-DMR-86-14003, and by the Division of Applied Sciences, Harvard University.

*Member, American Ceramic Society.

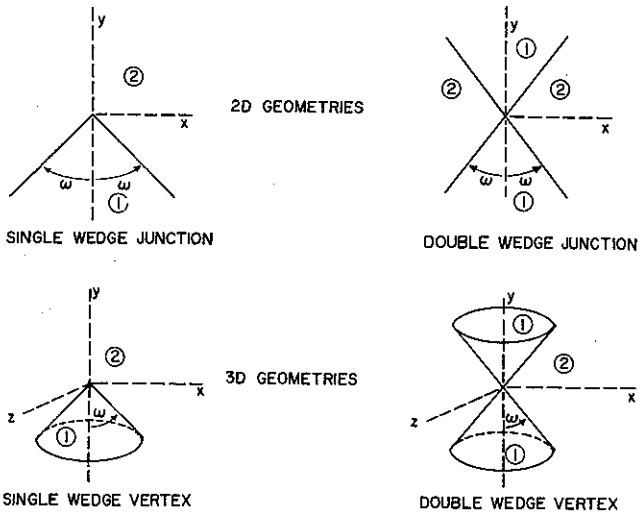

Fig. 1. Wedge geometries.

In each instance, the elasticity is isotropic and homogeneous with Young's modulus E and Poisson's ratio ν. The thermal expansion behavior is also taken to be isotropic and homogeneous in each region. Let $\varepsilon^T \equiv \Delta\alpha\Delta T$ be the transformation strain deriving from the thermal expansion mismatch $\Delta\alpha = \alpha_1 - \alpha_2$, where regions 1 and 2 are shown in Fig. 1. The equivalent transformation strain in region 1 is $\varepsilon_{ij}^T = \varepsilon^T\delta_{ij}$. Using well-known methods in elasticity theory, one can derive an integral representation for the stresses induced by the transformation strains. The singular behavior in the vicinity of the junction or vertex can be extracted analytically. For the 2D single wedge geometry, the normal stress acting on the plane extending from the wedge tip is given by $(y > 0)$

$$\sigma_{xx}(0,y) \to \frac{1}{2\pi}\frac{E\varepsilon^T}{1-\nu}\sin 2\omega \ln (cL/y) \tag{1}$$

where ω is the half-angle of the wedge, L is a length quantity (such as the size of the wedge or the grain size in a polycrystal), and c is a dimensionless numerical factor undetermined by the asymptotic analysis. The corresponding result for the 3D single conical wedge is found to be

$$\sigma_{xx}(0,y) = \frac{1}{16}\frac{E\varepsilon^T}{1-\nu}(\cos\omega - \cos 3\omega)\ln (cL/y) \tag{2}$$

For the 2D junction the maximum amplitude of the singularity occurs when $\omega = 45°$ and the associated numerical factor multiplying $[E\varepsilon^T/(1-\nu)]\ln(cL/y)$ in Eq. (1) is $1/(2\pi)$. For the 3D vertex the maximum amplitude occurs when $\omega \cong 55°$ with a corresponding numerical factor 0.096 in Eq. (2). Thus, the ratio of the 2D to 3D numerical factors is 1.65. The constant c will differ from the 2D to the 3D geometry, but the dependence of the stresses on c is weak by virtue of its appearance in the logarithm. Consequently, if these geometries can be regarded as representative, it appears that, in the absence of elastic anisotropy mismatch, stress amplification along a junction is more severe than at the vertex.

III. Elastic Moduli Mismatch and Elastic Anisotropy Mismatch

In this section results are presented for the exponent of the stress singularity at junctions and vertices where materials come together with either different isotropic moduli or with a given elastic anisotropy with different orientations. Attention is directed to the geometries of Fig. 1. The 2D junction problems are analyzed as plane strain; the 3D vertex problems have axial symmetry and the fields sought are limited to be axisymmetric.

In each example considered here the dominant asymptotic stress field in the vicinity of the junction or vertex is of the form

$$\sigma_{ij} = kr^{-s}\tilde{\sigma}_{ij}(\theta) \tag{3}$$

where r is the distance from the common point and θ is either the polar angle or the azimuthal angle. The exponent s and the field $\tilde{\sigma}_{ij}(\theta)$ are the eigenvalue and the eigenfunction, respectively, of an eigenvalue problem obtained from the field equations and depending on the moduli and geometry. In the examples presented below, s turns out to be real. Details of the solution procedure will not be given here since they are fairly standard. The numerical scheme employed is essentially identical to that outlined in an earlier paper on 2D problems.[5] For the case of the 3D single wedge geometries with different isotropic elastic moduli, we have checked our numerical results against previous results of this type.[6,7]

First, consider examples of *moduli mismatch* where the material in region 1 of Fig. 1 is isotropic with shear modulus μ_1, and Poisson's ratio ν_1, while these quantities are μ_2 and ν_2 in region 2. The plots of s in Figs. 2 and 3 were computed with $\nu_1 = \nu_2 = 0.3$ and $\omega = 30°$. The double wedge geometry has more singular stresses (i.e., larger s) than the single wedge in all cases. The strongest singularities occur when $\mu_1 > \mu_2$, and for each of the two geometries the vertex singularity is stronger than the corresponding junction singularity. When μ_1 is sufficiently large compared to μ_2, the double wedge geometry has an exponent larger than ½. Elastic moduli mismatch in combination with special geometric configurations can lead to *super singularities* at a wedge which are stronger than the $r^{-1/2}$ singularity at the tip of a crack.

Super singularities are potent sites for microcrack nucleation as can be seen from the following general form of the energy release rate of a microcrack flaw emerging from the vertex. Let $\tilde{\sigma}_{ij}$ in Eq. (3) be dimensionless so that k has dimensions of (stress) × (length)^s. If a is the characteristic length of a microcrack flaw emerging from the vertex and if the flaw is sufficiently small such that it is embedded within the region dominated by Eq. (3), then dimensional considerations require that the energy release rate at any point on the edge of the microcrack be of the form

$$\mathcal{G} \propto k^2 a^{1-2s} \tag{4}$$

Thus, if $s > ½$, $\mathcal{G}$ becomes unbounded as $a \to 0$. In principle, an arbitrarily small flaw will nucleate a microcrack, assuming it can be treated within the continuum mechanical framework. Further consequences will be discussed in subsequent sections.

The results shown in Figs. 2 and 3 are not strongly dependent on the wedge half-angle ω. This can be seen in Fig. 4, where the singularity exponent is plotted as a function of ω for two values of μ_1/μ_2 for the double wedge vertex geometry.

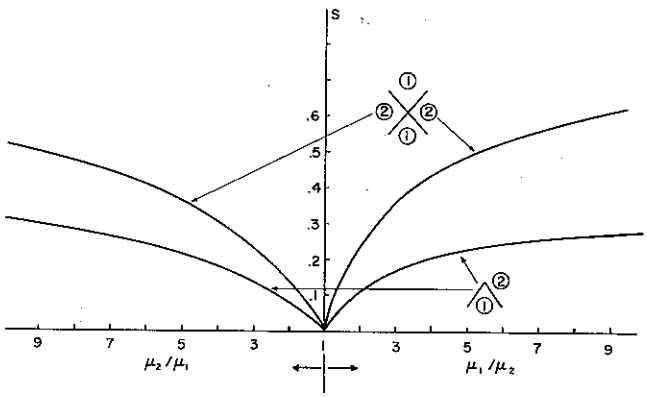

Fig. 2. Singularity exponent for 2D wedge junction geometries with elastic moduli mismatch ($\omega = 30°$).

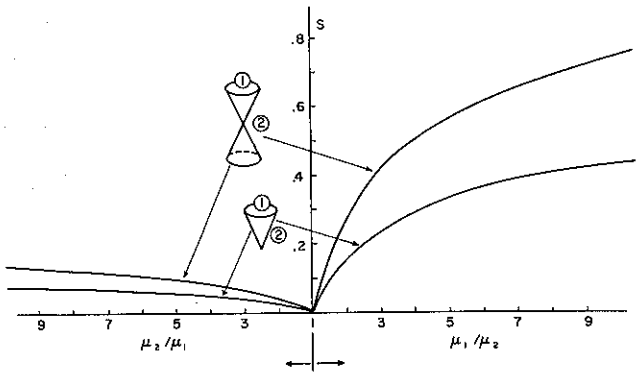

Fig. 3. Singularity exponent for 3D wedge vertex geometries with elastic moduli mismatch ($\omega = 30°$).

Now consider an example of *elastic anisotropy mismatch* where the elastic properties in regions 1 and 2 are identical but the principal axes of anisotropy are oriented differently. Specifically, consider the 3D vertex geometries of Fig. 1 and a transversely isotropic material whose axis of symmetry is the 1-axis. The elastic moduli ($\sigma_{ij} = L_{ijkl}\varepsilon_{kl}$) of a transversely isotropic material can be specified in terms of five independent parameters—α, β, γ, δ, and ε—such that in the axes of transverse isotropy

$$\begin{aligned} L_{1111} &= \gamma \\ L_{1122} &= L_{1133} = \beta \\ L_{2222} &= L_{3333} = \alpha + \delta \\ L_{2233} &= \alpha - \delta \\ L_{1212} &= L_{1313} = \varepsilon \\ L_{2323} &= \delta \end{aligned} \tag{5}$$

where α, δ, ε, and $\gamma - \beta^2/\alpha$ are all positive if the moduli are positive definite. In the limit of isotropy

$$\begin{aligned} \alpha &= \xi + \frac{1}{3}\zeta \\ \beta &= \xi - \frac{2}{3}\zeta \\ \gamma &= \xi + \frac{4}{3}\zeta \\ \delta &= \varepsilon = \zeta \end{aligned} \tag{6}$$

where $\xi = E/[3(1 - 2\nu)]$ and $\zeta = E/[2(1 + \nu)]$.

The moduli are oriented in a way which preserves axial symmetry about the y axis. In region 1 the axis of transverse isotropy, the 1-axis, is aligned parallel to the y axis. In region 2 the 1-axis of the material is aligned at every point in the planar-radial direction perpendicular to the y axis (i.e., in the R direction where $R = (x^2 + z^2)^{1/2}$), as depicted in the insert in Fig. 5. Thus, in region 2 the orientation of the axis of transverse isotropy varies with the circumferential angle to preserve axial symmetry. In an approximate way, this elastic anisotropy mismatch models a vertex where transversely isotropic grains meet.

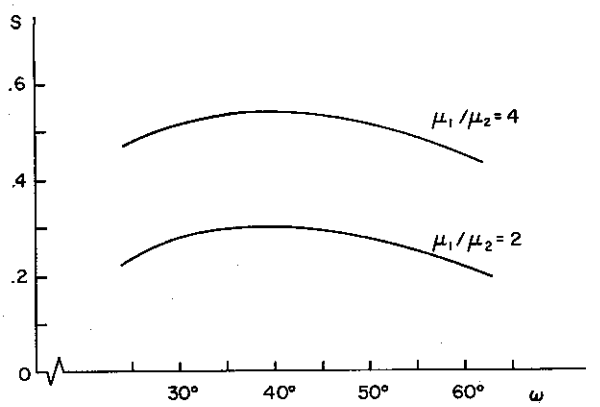

Fig. 4. Dependence of singularity exponent on vertex angle ω for 3D double wedge vertex.

The example in Fig. 6 shows the dependence of the exponent s of the dominant singularity on α when β, γ, δ, and ε are held fixed. The reference values, used in the next example as well, are taken as the isotropic limit Eq. (6) with $\nu = 0.3$ and are denoted by α^0, β^0, γ^0, δ^0, and ε^0. Thus in Fig. 6 only α is varied. Note that both L_{2222} and L_{2233} depend on α. The abscissa in Fig. 5 is taken as L_{2222}/L^0_{2222} where L^0_{2222} is the reference value. The wedge angle is $\omega = 45°$. Two features of this plot stand out. The singularity exponent s becomes appreciable for relatively modest levels of anisotropy, with s exceeding ½ for values of L_{2222}/L^0_{2222} less than 0.63 or 0.58 depending on whether the vertex is a double or single wedge. Secondly, unlike the results for the moduli mismatch, the dependence of s on which of the two geometries is considered is relatively weak with the double wedge vertex only slightly more singular than the single wedge vertex.

The dependence of s on γ is shown in Fig. 5. In this case only L_{1111} varies with γ when α, β, δ, and ε are held at their reference values, and the abscissa in Fig. 5 is taken to be L_{1111}/L^0_{1111} where L^0_{1111} is the reference value from Eq. (6) with $\nu = 0.3$. Only the range $L_{1111}/L^0_{1111} \geq 1$ is shown since then the singularity is the strongest. As in the previous example, the double wedge vertex is only slightly more singular than the single wedge vertex. Additional calculations have been performed with other values of ω and by varying other moduli parameters. The variations of s shown in Figs. 5 and 6 are representative.

IV. Exponents of Stress Singularities at Vertices of Grains in Polycrystals

The dominant singular stress field at a true 3D vertex of a polycrystal where homogeneous anisotropic grains of different orientation come together is of the form

$$\sigma_{ij} = kr^{-s}\tilde{\sigma}_{ij}(\phi, \theta) \tag{7}$$

where r, ϕ, and θ are spherical coordinates with r as the distance from the vertex and where s is the stress exponent.

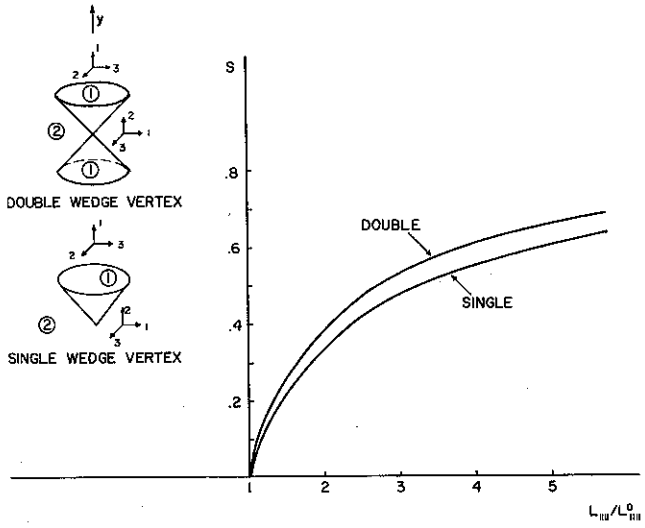

Fig. 5. Singularity exponent for elastic anisotropy mismatch. See text for description of moduli and mismatch.

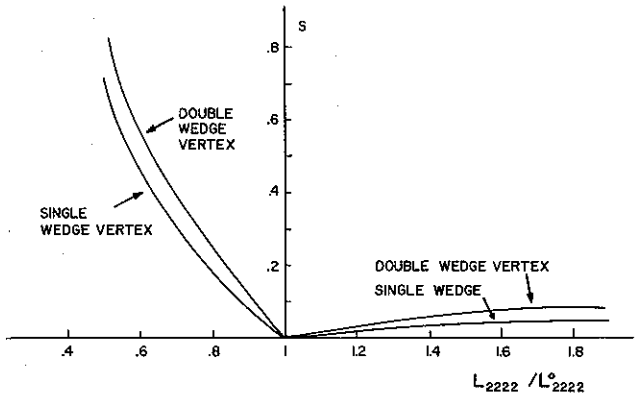

Fig. 6. Singularity exponent for elastic anisotropy mismatch. See text for description of moduli and mismatch.

Each junction is taken to be a straight line emerging from the vertex. If one imagines a sphere of radius r centered at the vertex, a junction is a point (ϕ, θ) on that sphere. The grain boundaries are curves connecting junction points on the sphere with each grain corresponding to a region on the sphere.

The equations of linear elasticity admit separated solutions of the form of Eq. (7). The equations governing the solution are a set of partial differential equations in ϕ and θ covering the sphere. The separated problem is a homogeneous eigenvalue problem with s as the eigenvalue. A numerical method has been developed, with details which will be published elsewhere, to solve for s and for the associated eigenfield $\tilde{\sigma}_{ij}(\phi, \theta)$. The method is based on a variational principle originally formulated by Bazant[8] and makes use of a "natural" finite-element grid covering the sphere; it has features in common with other methods developed to analyze 3D singularities.[9,10] The method is capable of solving for complex s. In most of the cases presented in this paper the most singular fields of interest are associated with an eigenvalue s which is real.

The examples considered in this section all involve grains of cubic crystals. Let

$$f = 2C_{44}/(C_{11} - C_{12}) \tag{8}$$

be the standard measure of the anisotropy of the single crystal. Let

$$\bar{\nu} = C_{12}/(C_{11} + C_{12}) \tag{9}$$

be the second nondimensional combination of the moduli which coincides with Poisson's ratio when $f = 1$ and, in general, is $-\varepsilon_2/\varepsilon_1$ for uniaxial stressing along the 1-direction of the crystal.

Attention will be confined to the classical vertex geometry where four grains of equal spherical area meet at a point.[11] The angle between the grain junction lines emerging from the vertex for a given grain is approximately 109°. The basic geometry and our labeling conventions are shown in Fig. 7. The grain junctions are specified by the four vectors $\mathbf{v}_1 = 2\sqrt{2}\mathbf{i} - \mathbf{k}$, $\mathbf{v}_2 = -\sqrt{2}\mathbf{i} + \sqrt{6}\mathbf{j} - \mathbf{k}$, $\mathbf{v}_3 = -\sqrt{2}\mathbf{i} - \sqrt{6}\mathbf{j} - \mathbf{k}$, and $\mathbf{v}_4 = \mathbf{k}$. Grain I has junctions $(\mathbf{v}_1,\mathbf{v}_2,\mathbf{v}_4)$; II has $(\mathbf{v}_1,\mathbf{v}_2,\mathbf{v}_3)$; III has $(\mathbf{v}_2,\mathbf{v}_3,\mathbf{v}_4)$; and IV has $(\mathbf{v}_1,\mathbf{v}_3,\mathbf{v}_4)$.

(1) Basic Symmetry A

The first example is one in which the (1,1,1) axis of each of the single crystals is aligned with the central axis of its grain. By central axis, we mean the line through the vertex which makes equal angles with the three junction lines of the grain. The crystal orientation in basic symmetry A is identical in each grain *relative to the grain* as shown in Fig. 7. For $f > 1$ the stresses are bounded at the vertex (i.e., real $s < 0$) until f is larger than about 15, which is beyond the range of interest. The dependence of s on f for $f < 1$ is shown in Fig. 8. The calculations were made with $\bar{\nu} = 0.3$ but additional calculations with other values of $\bar{\nu}$ indicated that s is independent of $\bar{\nu}$.

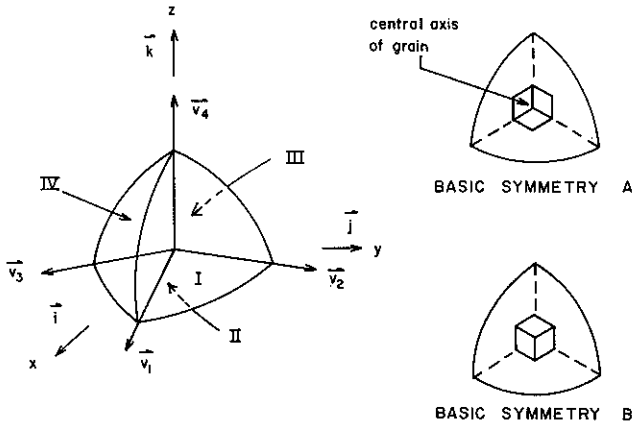

Fig. 7. Vertex geometry. The cubic crystals in basic symmetries A and B have a (1,1,1) direction parallel to the central axis of the grain and their cube edges oriented relative to the grain as shown when viewed along the central axis.

(2) Basic Symmetry B

In this case the (1,1,1) axis of the crystal in each grain is also aligned with the central axis but now each grain is rotated about the central axis by 60° relative to its orientation in basic symmetry A, as shown in Fig. 7. For $f > 1$, the real part of s is negative so that the stresses are bounded at the vertex. For $f < 1$, the real part of s is positive, implying singular stresses, but the imaginary part of s is of comparable magnitude to the real part. Thus the singularity for this case is of the more complicated oscillatory type.

(3) Example for Cubic ZrO_2 ($f = 0.281, \bar{\nu} = 0.164$)

The result for the basic symmetry of Fig. 8 applies to ZrO_2 with $f = 0.281$, i.e., $s \cong 0.22$. Now suppose the basic symmetry is broken by rotating the crystals in grains I and IV about their (1,1,1) axis which is aligned with the central grain axis. Let the rotation of these crystals be ψ in the sense shown in Fig. 9. By rotating the crystals in both grains I and IV in this manner the symmetry of the problem with respect to the x–z plane is preserved, and this symmetry is exploited in reducing the size of the computation. The dependence of s on ψ is shown in Fig. 9. The most singular case is that of basic symmetry.

(4) Case C

In this case the [001] direction of the crystal in each grain coincides with the central axis. The [100] direction is taken to be parallel to the x–y plane in each grain. This prescribes the orientations for the crystals in grains I, III, and IV. In

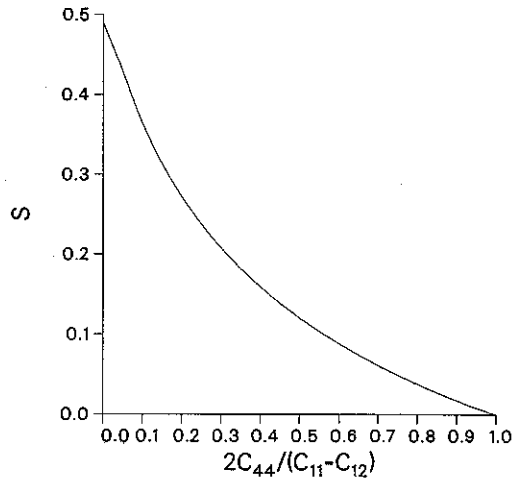

Fig. 8. Singularity exponent for four-grain vertex with cubic crystals oriented with basic symmetry A.

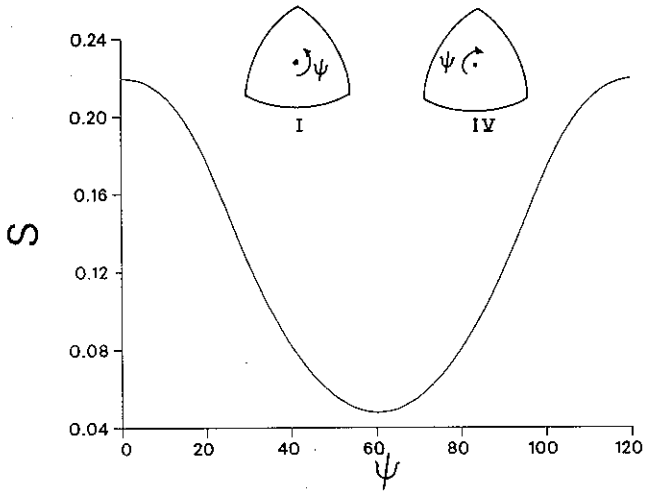

Fig. 9. Singularity exponent for four-grain vertex with cubic crystals with anisotropy of ZrO_2. With $\psi = 0$, crystals have basic symmetry A. Grains I and IV are rotated about the central axis in the sense shown.

grain II, the [100] direction is taken to be parallel to the y direction. Symmetry with respect to the x–z plane exists for this case too.

Now, the stresses are bounded at the vertex when $f < 1$ and unbounded when $f > 1$. A plot of s (which is real) vs $1/f$ for $f > 1$ is shown in Fig. 10. The results are independent of $\bar{\nu}$. Included in Fig. 10 are the results of a 2D plane strain calculation for a three-grain junction taken from Ref. 5.* In the 2D calculation the [001] axis of the crystal bisects the facet planes of each grain, as shown in the insert of Fig. 10, and the [100] axis in each grain is aligned parallel to the 2D junction line which is perpendicular to the plane of the figure. The 3D vertex singularity is stronger than the 2D junction singularity, although orientation of the crystals in the 2D junction does not correspond precisely to any of the junctions of the 3D vertex.

(5) Rotation from Case C

With case C as reference, rotate the crystals in grains I and IV about their [001] direction (i.e., about the central axis) by an amount ψ with the sense shown in the inserts in Fig. 11. Symmetry with respect to the x–z plane is still preserved. The variation of s and ψ is shown in Fig. 11 for two values of f, including the extreme limit of anisotropy, $f \to \infty$. In this

*A different measure of elastic anisotropy of cubic single crystals was used in Ref. 5. The present choice of f, which is the standard measure, is much to be preferred since s depends on f, independent of $\bar{\nu}$. The choice in Ref. 5 resulted in s depending on the two nondimensional moduli measures.

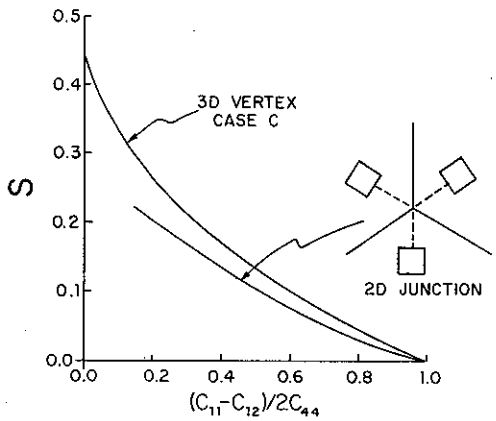

Fig. 10. Singularity exponents for four-grain vertex, case C, and for three-grain, 2D junctions.

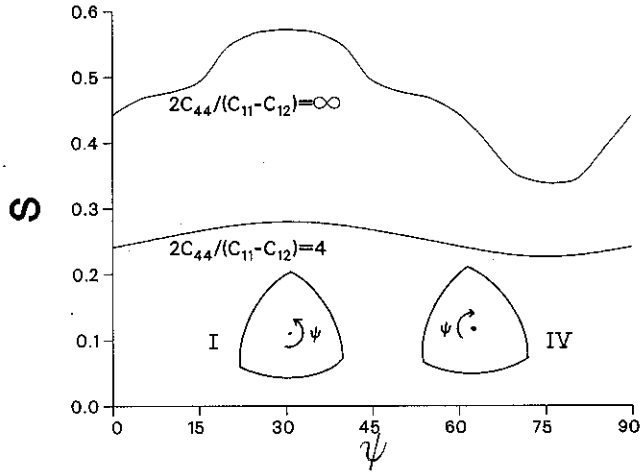

Fig. 11. Singularity exponent for four-grain vertex where grains I and IV are rotated from their reference orientations in case C in the sense shown.

example the dependence of s on ψ is not very strong. There is a range of orientations where the most highly anisotropic crystals give rise to s values greater than ½. Thus, in principle, super singularities are possible at some vertices of cubic polycrystals. However, the present study suggests that singularities that strong are not likely in cubic materials with moderate levels of elastic anisotropy. It must be recognized that the present study is far from being exhaustive in that it has been limited to a single vertex geometry and to only a relatively few orientation mismatches between cubic crystals. Consideration of other geometries and crystal classes may produce stronger singularities.

V. Microcracking at a Vertex with Elastic Anisotropy and Thermal Expansion Mismatches

Numerical calculations based on the finite-element method have been used to compute the energy release rate $\mathcal{G}$ of a microcrack emerging from a 3D vertex. The axisymmetric geometry is shown in the insert in Fig. 12 along with its transverse section. An axisymmetric conical crack of slant length a lying on the interface between regions 1 and 2 exists at the vertex. The moduli in each region have transverse isotropy as specified by Eqs. (5). The arrangement of anisotropy mismatch is identical to that in Section III with the 1-axis aligned with the axis of symmetry in region 1 and the 1-axis directed in the planar radial direction perpendicular to the axis of symmetry in region 2. To mimic the behavior at a typical vertex joining grains in a polycrystal, special cell model boundary conditions are applied. The cylindrical sides are free of shear traction but are constrained to remain straight with zero net normal traction. The top and bottom faces are also free of shear traction and are constrained to remain flat with net normal traction equal to the applied overall tensile stress $\bar{\sigma}$. When the model is stressed by thermal expansion mismatch, the average normal traction on the ends is required to vanish. Some details of the finite-element modeling are discussed in the Appendix, including the methods used to evaluate the energy release rate of the crack.

The first numerical example in Fig. 12 shows the effect of overall stress $\bar{\sigma}$ on the energy release rate of the crack when there is no thermal expansion mismatch. In this figure, the nondimensional release rate, $\mathcal{G}L^0_{111}/(\bar{\sigma}^2 H)$, is plotted as a function of a/H for a number of different moduli corresponding to varying α in Eqs. (5) with β, γ, δ, and ε fixed at their reference values in Eqs. (6) with $\nu = 0.3$. The exponent of the stress singularity at the vertex in the absence of the microcrack ($a = 0$) for this example was presented in Fig. 5 and the numerical values of s are included in Fig. 12. To the

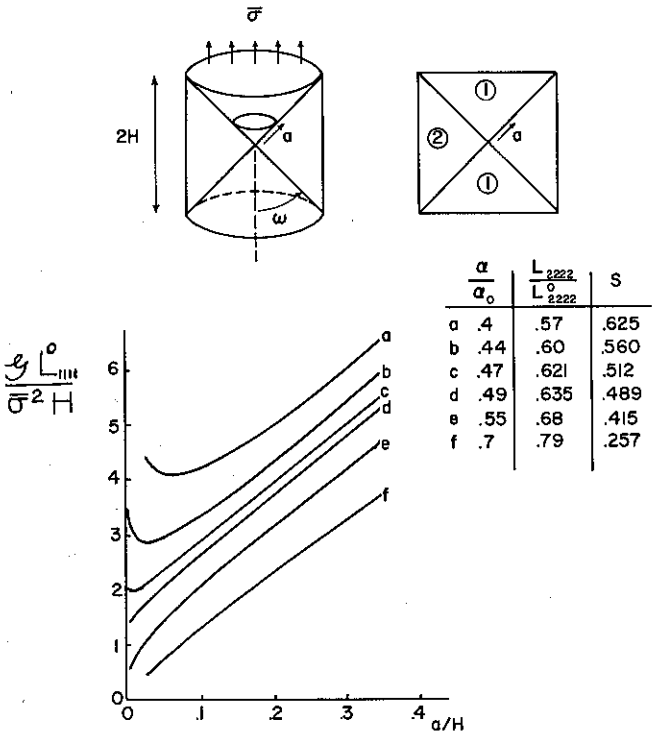

$\frac{a}{a_0}$	$\frac{L_{2222}}{L^0_{2222}}$	S
a .4	.57	.625
b .44	.60	.560
c .47	.621	.512
d .49	.635	.489
e .55	.68	.415
f .7	.79	.257

Fig. 12. Normalized energy release rate for a conical microcrack emerging from a double wedge vertex ($\omega = 45°$). See text for specification of elastic anisotropy mismatch.

extent that the finite-element scheme can resolve the behavior of the crack for very small a, the results of Fig. 12 display the transition noted in connection with Eq. (4), where $\mathcal{G}$ is either zero or unbounded as $a \to 0$, depending on whether s is smaller or larger than ½. Moreover, the finite-element results appear to be remarkably in accord with the vertex singularity analysis in this respect with the transition occurring somewhere between $\alpha/\alpha_0 = 0.49$ ($s \cong 0.49$) and $\alpha/\alpha_0 = 0.47$ ($s \cong 0.51$).

The second numerical example illustrates the effect of stressing due to thermal expansion anisotropy mismatch in combination with elastic anisotropy mismatch with no overall stressing ($\bar{\sigma} = 0$). The elastic moduli are the same as those used in the previous example. The nonzero coefficients of thermal expansion in the principal axes of the material are α_{11} and $\alpha_{22} = \alpha_{33}$ and we take $\Delta\alpha \equiv \frac{1}{2}(\alpha_{11} - \alpha_{22})$. The thermal anisotropy mismatch is due to the differing orientations from region 1 to region 2 (and to the circumferential variation of the 1-axis in region 2). Curves of the normalized energy release rate $\mathcal{G}/[\Delta\alpha\Delta T)^2 L^0_{1111} H]$ are shown in Fig. 13, where ΔT is the temperature drop measured from the zero stress state. The transition between bounded and unbounded $\mathcal{G}$ as $a \to 0$ again correlates with the exponent s of the vertex singularity, although the resolution of the behavior for small a is not sufficiently sharp when $\alpha/\alpha_0 = 0.49$. Clearly, the singularity associated with the elastic anisotropy mismatch dominates the relatively weaker logarithmic singular behavior associated with a purely thermal expansion anisotropy mismatch. The situation in 2D is similar in this respect.[5]

A comparison between the 3D model and the corresponding 2D plane strain model is shown in Fig. 14. The 2D model has the same type of cell model boundary conditions as the 3D model. The 1-axis of the moduli is aligned with the y axis in region 1 and with the x axis in region 2. The examples in Fig. 14 were computed with $\alpha/\alpha_0 = 0.55$ (corresponding to $(L_{2222}/L^0_{2222} = 0.679)$ and $\omega = 45°$. The exponent for the double wedge vertex is $s \equiv 0.41$, only slightly below the transition. In this example the energy release rate for the vertex crack increases much more rapidly than for the junction when a is small, and the peak value of $\mathcal{G}$ for the vertex crack is more

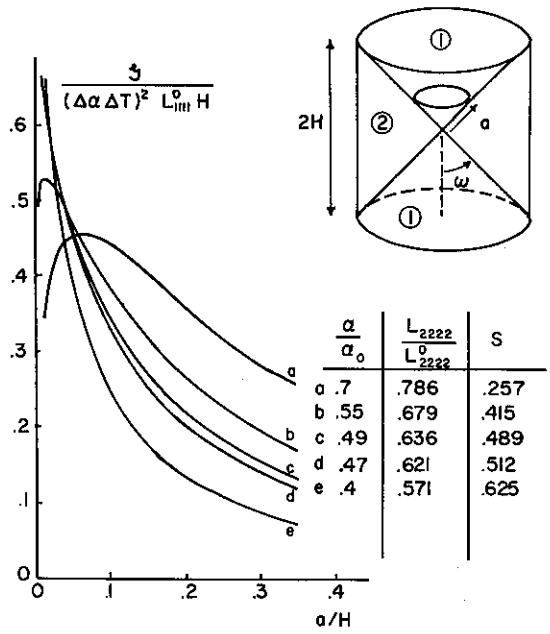

$\frac{a}{a_0}$	$\frac{L_{2222}}{L^0_{2222}}$	S
a .7	.786	.257
b .55	.679	.415
c .49	.636	.489
d .47	.621	.512
e .4	.571	.625

Fig. 13. Normalized energy release rate for a conical microcrack emerging from a double wedge vertex ($\omega = 45°$). See text for specification of elastic anisotropy and thermal expansion mismatches.

than twice that for the junction. Included as a dashed line curve in Fig. 14 is the result of a computation for a doubly conical crack which is symmetric with respect to $y = 0$. The energy release rate for the symmetric crack is only slightly smaller than that for the single conical crack.

VI. Discussion

Grain-boundary vertices and junctions become potent sites for microcrack nucleation when elastic anisotropy is appreciable. Generally, vertices concentrate the stress more than junctions. Under loading due to thermal expansion mismatch, microcracks nucleated at vertices will tend to be highly stable following nucleation with dimensions which are a very small function of the grain diameter, as can be seen in Figs. 13 and 14. The greater the elastic anisotropy mismatch, the more

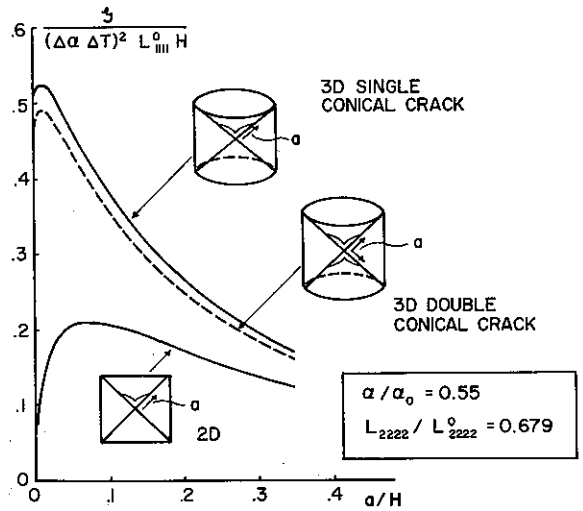

Fig. 14. Comparison of normalized energy release rates for microcracks emerging from a 3D vertex with that for a microcrack emerging from a 2D junction ($\omega = 45°$). See text for specification of elastic anisotropy and thermal expansion mismatches.

sharply the drop in the energy release rate with crack advance for a microcrack emerging from the vertex. In the extreme when super singularities exist, stable microcracks are nucleated by arbitrarily small flaws. When overall applied stress is then superimposed onto the residual stresses due to thermal expansion mismatch, the initial advance of the microcracks is also more likely to be stable when the residual fields are highly focused at the vertices at junctions. This is simply because the crack driving force, which is made up of contributions from the overall stress and the residual stress, will only decrease with crack advance under constant overall stress if the contribution due to the residual stress falls off sharply. Thus, heterogeneity due to elastic anisotropy mismatch in brittle polycrystalline solids promotes the nucleation of stable microcracks. Such heterogeneity undoubtedly plays a role in mechanisms of deformation and toughening involving microcracking.

APPENDIX

Numerical Analysis for Grain-Boundary Microcracks

The analyses for a microcrack at a grain vertex are based on the assumption of periodicity of the grain distribution, so that symmetry conditions are prescribed at the edges of the region analyzed (see Fig. 12). Thus, at the ends the normal displacements are constant and there are no shear stresses, while the average normal stress $\bar{\sigma}$ is prescribed. On the cylindrical surface (in the case of axisymmetry), the radial displacements are constant with no shear stresses, and the average transverse stress is prescribed to be zero.

An approximate solution is obtained by the finite-element method. Eight noded isoparametric elements are used, and the mesh is chosen such that no element crosses a grain boundary. The mesh is strongly refined near the crack tip, with several rings of small elements around the tip. The 10 elements in the first ring around the crack tip are wedge shaped, so that one side is collapsed to a point, and the 21 nodes meeting at the crack tip are tied together as a single node.

The energy release rate $\mathcal{G}$ (per unit length of the crack front) is determined by the stiffness derivative finite-element technique.[12] The expression for the derivative of the total potential energy with respect to crack advance involves derivatives of element stiffnesses and load term (e.g., load terms resulting from thermal expansion), and these derivatives are determined by a finite-difference approximation, based on perturbations of the local mesh near the crack tip.

Also, the J-integral is evaluated on a number of contours that follow the rings of elements around the crack tip. For planar conditions the J-integral is path independent, and this also applies to inhomogeneous materials as long the inhomogeneity is independent of the coordinate parallel with the crack. For the axisymmetric crack configuration there is no path independence, and the applicability of the J-integral is limited to contours of very small radius around the crack tip; for isothermal conditions the actual strain energy density expression, accounting for thermal expansion, is used in the J-integral.[13]

In the analyses carried out here the values of the energy release rate obtained by the J-integral agree with the values determined by the stiffness derivative technique within 2% to 3%.

References

[1]D. R. Clarke, "Microfracture in Brittle Solids Resulting from Anisotropic Shape Changes," *Acta Metall.*, **28**, 913–24 (1980).

[2]A. G. Evans, "Microfracture from Thermal Expansion Anisotropy—I. Single Phase Systems," *Acta Metall.*, **26**, 1845–53 (1978).

[3]J. T. Fredrich and T.-F. Wong, "Micromechanics of Thermally Induced Cracking in Three Crustal Rocks," *J. Geophys. Res., B*, **91** [12] 12,743–12,764 (1986).

[4]R. W. Rice and R. C. Pohonka, "Grain-Size Dependence of Spontaneous Cracking in Ceramics," *J. Am. Ceram. Soc.*, **62** [11–12] 559–63 (1979).

[5]V. Tvergaard and J. W. Hutchinson, "Microcracking in Ceramics Induced by Thermal Expansion or Elastic Anisotropy," *J. Am. Ceram. Soc.*, **71** [3] 157–66 (1988).

[6]Z. P. Bazant and L. M. Keer, "Singularities of Elastic Stresses and of Harmonic Functions at Conical Notches or Inclusions," *Int. J. Solids Struct.*, **10**, 957–64 (1974).

[7]L. M. Keer and K. S. Parihar, "Elastic Stress Singularities at Conical Inclusions," *Int. J. Solids Struct.*, **14**, 261–63 (1978).

[8]Z. P. Bazant, "Three-Dimensional Harmonic Functions Near Termination or Intersection of Gradient Singularity Lines: A General Numerical Method," *Int. J. Eng. Sci.*, **21**, 221 (1974).

[9]Z. P. Bazant and L. F. Estenssoro, "Surface Singularity and Crack Propagation," *Int. J. Solids Struct.*, **15**, 405 (1979).

[10]N. Somaratna and T. C. T. Ting, "Three-Dimensional Stress Singularities in Anisotropic Materials and Composites," *Int. J. Eng. Sci.*, **24**, 1115 (1986).

[11]C. S. Smith, "Grain Shapes and Other Metallurgical Applications of Topology"; pp. 65–113 in Metal Interfaces. American Society for Metals, Cleveland, OH, 1952.

[12]D. M. Parks, "A Stiffness Derivative Finite Element Technique for Determination of Crack Tip Stress Intensity Factors," *Int. J. Fract.*, **10**, 487–502 (1974).

[13]C. F. Shih, B. Moran, and T. Nakamura, "Energy Release Rate Along a Three-Dimensional Crack Front in a Thermally Stressed Body," *Int. J. Fract.*, **30**, 79–102 (1986). □